Gondwana Research 19 (2011) 372–383

Contents lists available at ScienceDirect

Gondwana Research

journal homepage: www.elsevier.com/locate/gr

Dynamic subsidence of Eastern Australia during the Cretaceous

Kara J. Matthews [a,*], Alina J. Hale [a], Michael Gurnis [b], R. Dietmar Müller [a], Lydia DiCaprio [a,c]

[a] EarthByte Group, School of Geosciences, The University of Sydney, NSW 2006, Australia
[b] Seismological Laboratory, California Institute of Technology, Pasadena, CA 91125, USA
[c] Now at: ExxonMobil Exploration Company, Houston, TX, USA

ARTICLE INFO

Article history:
Received 16 February 2010
Received in revised form 25 June 2010
Accepted 28 June 2010
Available online 13 July 2010

Keywords:
Geodynamic modelling
Subduction
Australia
Cretaceous
Tectonic subsidence
Basins

ABSTRACT

During the Early Cretaceous Australia's eastward passage over sinking subducted slabs induced widespread dynamic subsidence and formation of a large epeiric sea in the eastern interior. Despite evidence for convergence between Australia and the paleo-Pacific, the subduction zone location has been poorly constrained. Using coupled plate tectonic–mantle convection models, we test two end-member scenarios, one with subduction directly east of Australia's reconstructed continental margin, and a second with subduction translated ~1000 km east, implying the existence of a back-arc basin. Our models incorporate a rheological model for the mantle and lithosphere, plate motions since 140 Ma and evolving plate boundaries. While mantle rheology affects the magnitude of surface vertical motions, timing of uplift and subsidence depends on plate boundary geometries and kinematics. Computations with a proximal subduction zone result in accelerated basin subsidence occurring 20 Myr too early compared with tectonic subsidence calculated from well data. This timing offset is reconciled when subduction is shifted eastward. Comparisons between seismic tomography and model temperature cross-sections, and an absence of subduction zone volcanism in eastern Australia in the Early Cretaceous provide support for the back-arc basin scenario.

1. Introduction

During the Cretaceous the paleogeography of eastern Australia was influenced by mantle dynamics. A vast inland sea dominated the eastern interior for 10 Myr (Exon and Senior, 1976), prior to the Aptian global sea-level rise. At this time shallow marine sediments were deposited in an extensive basin system (~1.7×10^7 km^2) that had formed in the Jurassic. As global sea-levels rose, reaching a maximum in the Late Cretaceous (Haq et al., 1987), this inland sea retreated to the north (Exon and Senior, 1976) and the continent became largely exposed (Veevers, 2006). Eastern Australian basins underwent inversion and wide-spread erosion at this time (Gallagher et al., 1994; Raza et al., 2009). This seemingly inconsistent history, leaving Australia's flooding record out of sync with eustatic sea-level changes, has been attributed to the eastward passage of the Australian plate over subducted oceanic lithosphere originating from a subduction zone that separated Eastern Gondwanaland from the paleo-Pacific Ocean (Panthalassa) (Russell and Gurnis, 1994; Gurnis et al., 1998; Waschbusch et al., 2009). Subducted slabs viscously drag down the overlying lithosphere (Hager, 1984) causing widespread time-dependent subsidence (Mitrovica et al., 1989; Gurnis, 1992). When subduction ended ~100 Ma, coinciding with a distinct change in the absolute velocity of the Australian plate (Müller et al., 2008a), subsidence was followed by uplift. Such vertical motions of the Earth's surface, attributed to the interaction of plate motions with the passage of density anomalies through the mantle, are termed 'dynamic topography'. Dynamic topography has contributed to Phanerozoic continental flooding (Gurnis, 1990), and recognizing its influence has helped reconcile discrepancies between continental records of sea-level fluctuations and eustatic sea-level curves (Lithgow-Bertelloni and Gurnis, 1997; Spasojević et al., 2008; DiCaprio et al., 2009).

While there exists strong evidence to support dynamic vertical motions of the Australian continent since the Mesozoic (Gallagher et al., 1994; Russell and Gurnis, 1994; Sandiford, 2007; DiCaprio et al., 2009; Waschbusch et al., 2009), a geodynamic model for eastern Australia that reconstructs Cretaceous basin subsidence consistent with geological data remains elusive. Additionally, the location of the subduction zone that formed the eastern plate boundary of Australia (as a part of Eastern Gondwanaland) during the Cretaceous is poorly constrained. This is despite considerable knowledge of the Paleozoic to Mid-Triassic evolution of Australia's eastern margin, and the New England Orogen that was active during this time (Cawood, 1982; Murray et al., 1987; Little et al., 1992; Betts et al., 2002; Jenkins et al., 2002). For example, remnants of Paleozoic convergent margin volcanism, are abundant along Australia's eastern margin when westward-dipping subduction was active (Leitch, 1975; Murray et al., 1987; Holcombe et al., 1997), however evidence from the Cretaceous is limited (e.g. fluvial deposits of volcanic detritus in eastern Australian basins, Veevers, 2006), and there remains much

* Corresponding author. Fax: +61 2 9351 2442.
E-mail address: kara.matthews@sydney.edu.au (K.J. Matthews).

1342-937X/$ – see front matter
doi:10.1016/j.gr.2010.06.006

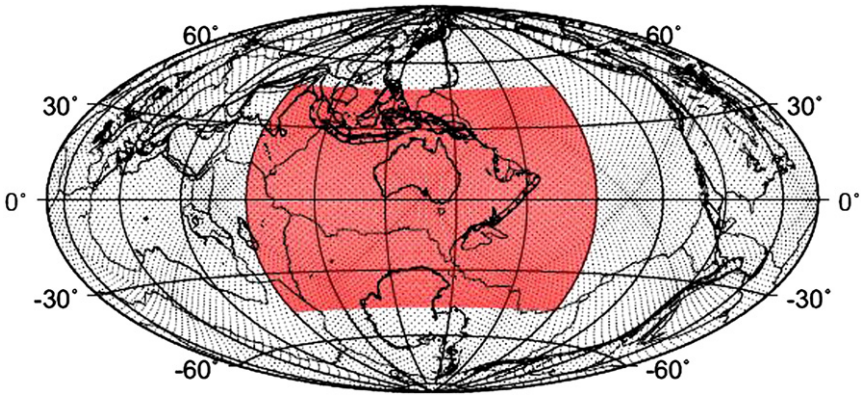

Fig. 1. Global map highlighting the location of the regional modelling domain (red) within the global domain (DiCaprio, 2009). Note: During the Mesozoic Australia was located at high latitudes and therefore a rotated reference frame is used to avoid regional mesh compression caused by the extremely reduced longitudinal distances near the poles.

debate over the origin of these volcanics, in terms of whether they are convergence or extension related. Furthermore subduction zones can be highly mobile, for example the Late Cretaceous and Tertiary subduction zones of the southwest Pacific underwent phases of trench roll-back, accommodating more than 1000 km, in some cases, of subduction zone retreat (Schellart et al., 2006). Additionally, it has been suggested that the subduction zone that formed Australia's eastern plate boundary from the Paleozoic to Triassic, underwent distinct episodes of advance and retreat (Holcombe et al., 1997; Jenkins et al., 2002). Therefore, a subduction zone located adjacent to Australia's continental margin during earlier periods does not preclude a large back-arc region, with subduction up to 1000 km further east during the Cretaceous.

We reconstruct the surface vertical motions attributed to mantle processes that are recorded in the sedimentary records of the Eromanga and Surat basins, to constrain the location of the subduction zone that paralleled Eastern Gondwanaland during the Cretaceous. The Jurassic–Cretaceous aged Eromanga and Surat basins in the eastern interior form the focus of our investigation as their formation and evolution are linked to the dynamics of the subduction zone that formed the eastern plate boundary of Australia. We have employed a workflow (DiCaprio, 2009) that links a mantle convection code (*CitcomS*) to software for plate kinematic reconstructions (*GPlates*).

2. Methods

Geodynamic models are able to simulate material deformation resulting from the interactions between the crust and mantle processes. We have produced a series of forward geodynamic models using the CIG finite element code *CitcomS version 3.0* (Zhong et al., 2000; McNamara and Zhong, 2004; Tan et al., 2006). *CitcomS* enables the solution of thermo chemical convection in a regional or a full spherical domain.

2.1. Model setup

Our geodynamic models couple a high-resolution 'regional' model domain, incorporating the Australian region, embedded within a low-resolution 'global' domain (Fig. 1). Coupled *CitcomS* solvers (Tan et al., 2006) allow temperature and velocity feedback between the two models. The temperature and velocity fields are continuous at the regional–global model boundary, whereby the global model provides the side and bottom boundary conditions for the regional model.

The global modelling domain is divided into 12 'caps', each extending to the core–mantle boundary. The regional mesh is bounded by constant latitude (47.5°N and 47.5°S) and longitude (60° and 210°), and extends to a depth of ~2230 km. Mesh geometries and surface resolutions are listed in Table 1. Both the global and regional mantle domains are divided into four radial layers, with varying temperature-dependent viscosities (Fig. 2):

$$\eta = \eta_0 \times \exp\left(\frac{E_\eta}{T + T_\eta} - \frac{E_\eta}{1 + T_\eta}\right), \quad (1)$$

where η_0 is the reference viscosity, E_η is a non-dimensional activation energy, T is temperature, and T_η is a constant. A lithosphere (0–100 km) is implemented with a high-viscosity to simulate mechanical rigidity. The remaining mantle is divided into upper mantle (100–410 km), transition zone (410–660 km) and lower mantle (660–2870 km). Variables held constant, and assimilated data sets are listed in Tables 2 and 3, respectively.

2.2. Initial conditions

To represent long-lived subduction of the Phoenix plate beneath Eastern Gondwanaland, that initiated in the Paleozoic, we introduce a slab that extends deep into the lower mantle (Fig. 3). The dip of the slab is set to 50° to a depth of 660 km, before vertically penetrating the lower mantle. Mantle material is prescribed the maximum non-dimensional temperature of 1, while the temperature of the slab decreases to 0, symmetrically from a minimum value in the centre (~0.5). A half-space cooling model, based on the age of oceanic crust at the trench, was used to define this temperature gradient in the slab (DiCaprio, 2009).

Additionally, the regional model is initiated with active tracers to provide buoyancy to the continental lithosphere and reduce the viscosity of the mantle wedge. During subduction, slab dehydration resulting from diagenesis and metamorphism, releases fluids into the mantle wedge (Tatsumi et al., 1983; Peacock, 1990; Ranero et al., 2003), reducing its viscosity (Billen and Gurnis, 2001; Baker-Hebert et al., 2009). A low viscosity mantle wedge can have an important influence on the evolution of the slab, especially its dip (Manea and Gurnis, 2007) and surface topography of the overlying plate (Billen and Gurnis, 2001; Billen et al., 2003). Tracers in the region of the

Table 1
Resolution of geodynamic models.

Model	Number of nodes			Surface resolution
	Latitude direction	Longitude direction	Z (radial) direction	
Global (per cap)	33	33	33	~200 km
Regional	257	257	65	~64 km (Long.)× ~40 km (Lat.)

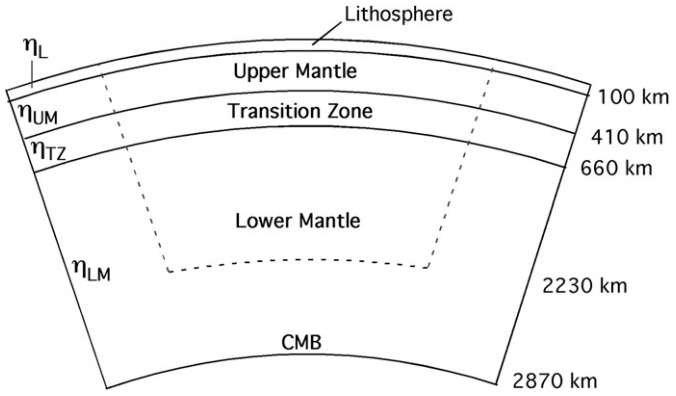

Fig. 2. Schematic illustrating the division of the modelling domains into 4 layers; Lithosphere (0–100 km), Upper Mantle (100–410 km), Transition Zone (410–660 km) and Lower Mantle 660–2870 km). Dashed lines define the regional embedded model. η_L—lower mantle viscosity, η_{UM}—upper mantle viscosity, η_{TZ}—transition zone viscosity and η_{LM}—lower mantle viscosity; values vary between models (see Eq. (1)). CMB—core–mantle boundary. (Not to scale).

mantle wedge reduce viscosity by a factor of 10 compared to the surrounding mantle material; consistent with the minimum decrease in mantle wedge viscosity from present-day gravity and topography above the mantle wedge (Billen and Gurnis, 2001).

2.3. Boundary conditions

Global and regional surface temperatures were computed from paleo-age-area distributions of the ocean floor (Müller et al., 2008b) in 1 Myr increments (Fig. 3). A half-space cooling model was used to derive a temperature from the lithospheric ages:

$$T^{HS} = T_S + (T_m - T_S) erf\left(\frac{z}{2\sqrt{kt}}\right), \quad (2)$$

where T_{HS} is the half-space temperature, T_S is the surface temperature (non-dimensionalised), T_m is the mantle temperature, t is age and z is depth.

These lithospheric temperatures were progressively assimilated into the convection models to a depth of 80 km:

$$T_{i+1} = aT_i + (1-a)T^{HS}_{i+1}; \quad \text{where} \quad a = \begin{cases} \frac{z}{z_p} & z < z_p \\ 1 & z \geq z_p \end{cases}, \quad (3)$$

where T_i is temperature at time step i, T^{HS}_{i+1} is the temperature derived from the half-space cooling equation at the given time step $(i+1)$, z is depth and z_p is the end depth of 80 km.

Plate velocities and plate boundary configurations in the regional and global meshes from 140 Ma were imposed as kinematic boundary conditions. These velocity data were determined using the plate reconstruction software *GPlates* (Boyden et al., in press), that allows for the high-resolution time-dependent evolution of plate polygons to define regions of differing velocities, as well as the generation of new plate boundaries (Gurnis et al., 2009). The plate polygons were updated at 1 Myr intervals, with velocities linearly interpolated at intervening times.

Table 2
Variables held constant between model runs.

Variable	Notation	Value
Reference mantle density	ρ_0	3500 kg/m^3
Gravity	g	10 m/s^2
Surface temperature	T_0	0°C
Temperature difference between the CMB and the surface	ΔT	1500°C
Radius	R_0	6371 km
Coefficient of thermal expansion	α	2×10^{-5} K^{-1}
Thermal diffusivity	κ	1×10^{-6} m^2/s
Reference viscosity	η_0	2×10^{21} Pa s

Table 3
Description of input files assimilated into *CitcomS* models.

Input file	Description	Model	Initial or boundary condition
Temperature	Describes temperature field with depth.	Global and regional	Initial condition
Tracer	Controls continental buoyancy and mantle wedge viscosity.	Regional	Initial condition
Velocity	Dictates plate motions and boundaries.	Global and regional	Boundary condition
Lithospheric age	Used to generate surface temperatures.	Global and regional	Boundary condition
Back-arc basin (temperature and velocity)	Forces slab down in to the mantle to ensure it does not surface.	Regional	Boundary condition

Dynamic topography is first computed on the top surface of the *CitcomS* mesh. Then, as the plates move with respect to this fixed mesh, we track the evolving dynamic topography of points fixed with respect to the moving plates (Gurnis et al., 2000).

We impose additional boundary conditions on the regional model to remove excessive slab suction so that the slabs descend more realistically into the upper mantle. Excessive slab suction is the result of low resolution models and viscosities in the mantle wedge which are not sufficiently small (Manea and Gurnis, 2006). Viscous flow in the mantle wedge, induced by plate motions, produce dynamic pressure forces along the slab (Stevenson and Turner, 1977; Tovish et al., 1978). Net negative pressure acting on the upper surface of the slab causes the slab dip angle to be reduced and can ultimately result in flat slab subduction. Following Christensen (1996) and Tan et al. (2002), a back-arc region is defined at mantle temperature (essentially removing the plate) with a trench perpendicular velocity, of a similar yet opposite magnitude to that of the converging oceanic plate (Fig. 3 – 140 Ma mantle cross-section and 88 km regional depth slice). These back-arc conditions are imposed for the first 20 Myr of the calculations.

2.4. Model runs

Mantle material properties and initial plate boundary configurations were varied in a preliminary series of model runs. Given the uncertainties in mantle viscosities, we consider a range of different parameters. We varied Rayleigh number (Ra), initial slab-mantle temperature contrast and viscosity of the upper mantle, transition zone and lower mantle. The Ra is defined as:

$$Ra = \frac{\rho_0 g_0 \alpha_0 \Delta T R_0^3}{\eta_0 \kappa_0}, \quad (4)$$

where ρ_0 is the reference density, g_0 is the reference gravity, α_0 is the reference thermal expansivity, ΔT is the temperature difference between the core–mantle boundary and the surface, R_0 is the Earth's radius, η_0 is the reference viscosity and κ_0 is the reference thermal diffusivity. It indicates the strength of heat transfer via convection.

To constrain the location of the subduction zone during the Cretaceous, two end-member scenarios were tested; one with subduction adjacent to the reconstructed eastern continental margin, and a second with subduction translated 23° further east (Tables 4 and 5) (Fig. 4).

2.5. Model validation

We validate the models by comparing them to two data sets. A tectonic subsidence analysis of borehole data, acquired along an east to west transect through the Eromanga and Surat basins, provides observational data with which to compare the predicted tectonic subsidence. Comparisons between seismic tomography and predicted present-day mantle temperature place further constraints on our models.

2.5.1. Borehole analysis

We backstripped 42 wells from the Eromanga and Surat basins following the methodology of Gallagher and Lambeck (1989) and Gallagher (1990) (Fig. 5). We use Gallagher's (1990) porosity depth relationship:

$$\phi(z) = \phi_o e^{-cz} \tag{5}$$

where ϕ is porosity, z is depth, ϕ_0 is porosity at z = 0 and c is a constant representing porosity decrease with depth. For simplicity it was assumed that there was no cementation. The errors associated with the assumed porosity–depth relationship were quantified by testing different values of ϕ_0 and c (Table 6). The tectonic subsidence was then calculated assuming Airy isostasy:

$$H_b = \{[(\rho_m - \rho_s)H_s - \rho_m H_{sl}] / (\rho_m - \rho_w)\} + H_w, \tag{6}$$

where H_b is the tectonic subsidence, H_s is the sediment thickness, H_{sl} is the difference between the sea-level at time of deposition and present sea-level, H_w is the water depth at time of deposition, ρ_m is mantle density, ρ_s is sediment density, and ρ_w is water density (i.e. seawater).

2.5.2. Seismic tomography analysis

We compared the ~0 Ma temperature fields of our models to a series of equivalent P- and S-wave whole-mantle seismic tomography models (Ritsema et al., 1999; Grand, 2002; Montelli et al., 2006; Simmons et al., 2007; Li et al., 2008). Vertical cross-sections were aligned east to west through the Eromanga and Surat basins (Fig. 6).

3. Model results

Consistent between all models is the immediate development of a band of negative topography west of the subduction zone. As Australia migrates east between 140 and 99 Ma this region of negative topography propagates westwards until it covers eastern Australia. The magnitude of the negative dynamic topography signal, and rate of subsidence are closely related to distance from the subduction zone, depth of the slab and mantle properties. When the slab is close to the surface the dynamic topography signal is stronger, and as the slab sinks deeper into the mantle the surface relatively uplifts as the negative signal diminishes in magnitude. The effects of dynamic corner flow on dynamic topography in eastern Australia are amplified when the arc corner is situated closer to the continent; tilting of the continent increases towards the subduction zone. When subduction is adjacent to the reconstructed margin, slab material is sinking at a shallower level in the mantle beneath eastern Australia compared to when the subduction zone is further east, so that the magnitude of negative dynamic topography is greater.

The present-day dynamic topography signal of the Australian region is dominated by active subduction to the north and east of Australia, however the effects of Cretaceous negative dynamic topography have not completely diminished. These results show that although dynamic topography is transient, its effect can persist for tens of millions of years. This further highlights that attributing absolute dynamic topography to one event can be complex, as a negative signal can have multiple sources of varying ages in regions of long-lived subduction.

3.1. Timing of accelerated subsidence in Eastern Australia

CitcomS and the backstripped borehole data reveal tectonic subsidence relative to an initial starting time (140 Ma). When subduction is located adjacent to the reconstructed margin at 140 Ma, Cretaceous subsidence accelerates at approximately 140 Ma, 20 Myr earlier than observed in the borehole record (Fig. 7). Shifting the subduction zone 23° east reconciles this timing mismatch (Figs. 8 and 9). Although the magnitude and rate of subsidence vary between models, the rate of subsidence consistently increases at ~120 Ma along the E–W transect of boreholes, in agreement with the local geology. However, tectonic subsidence analyses of borehole data from the Eromanga Basin also reveal a prominent increase in subsidence at ~100 Ma, following the more gentle acceleration at 120 Ma. Neither series of *CitcomS* models presently capture this second pulse of subsidence. Rather the Slab23E series of models predicts the initiation of uplift at this time.

3.2. Magnitude and rate of accelerated subsidence

Mantle material properties influence how rapidly a basin subsides. By increasing the Rayleigh number (Ra), analogous to a smaller viscosity or higher temperature mantle, we find that the slab encounters less resistance, and imparts more of a drag on the overlying surface as it descends. As a result the model run with $Ra = 2.7152 \times 10^8$ (double the reference Ra) results in the maximum subsidence signal of all the model runs (model RM_4 – Fig. 7).

Smaller absolute subsidence results from reducing Ra (model RM_5 – Fig. 7), or having a weaker upper mantle (model RM_2 – Fig. 7). A mantle with reduced Ra is more resistive to the descent of the slab. When convection is weaker the subducting slab has a smaller down-going velocity, resulting in diminished surface subsidence. Although the downward velocity of the slab is larger with a lower viscosity upper mantle (η_{UM}), the stresses on the surface from the slab are reduced. In higher viscosity regions the surface stresses are larger, and although the downward velocities may be smaller with higher η_{UM} and η_{LM}, the former effect dominates and subsidence is greater at the surface (models RM, RM_1 and RM_3 – Fig. 7).

A similarity between all models is that the timing of increased subsidence rates occurs simultaneously in the Surat and Eromanga basins, however the magnitude of subsidence is larger and more laterally variable when subduction is adjacent to the reconstructed margin (Fig. 7). This is likely because the slab is closer to the surface, and it is positioned at a steep angle when below the basins. When subduction is located further east, the slab is deeper in the mantle and lying at a relatively shallow angle by the time Eastern Australia passes over. Consistent between all models, is that the rate of subsidence in this episode is similar from east to west, with a slight increase in the east.

In order to improve the rates of subsidence in the basins, models with subduction shifted east were tested (Fig. 8). Increasing viscosities in the upper mantle, transition zone and lower mantle, while maintaining the same viscosity ratio as model Slab23E_RM (model Slab23E_1 – Table 5), produces a better fit between the observed and predicted rates of subsidence from 140 Ma. From Fig. 10 it can be seen that the slopes are comparable.

3.3. Present-day temperature field

S- and P-wave seismic tomography models for the southwest Pacific (Ritsema et al., 1999; Grand, 2002; Montelli et al., 2006; Simmons et al., 2007; Li et al., 2008) reveal high velocity material extending from the upper mantle through the transition zone to deep in the lower mantle beneath eastern Australia (Fig. 6). There is also a

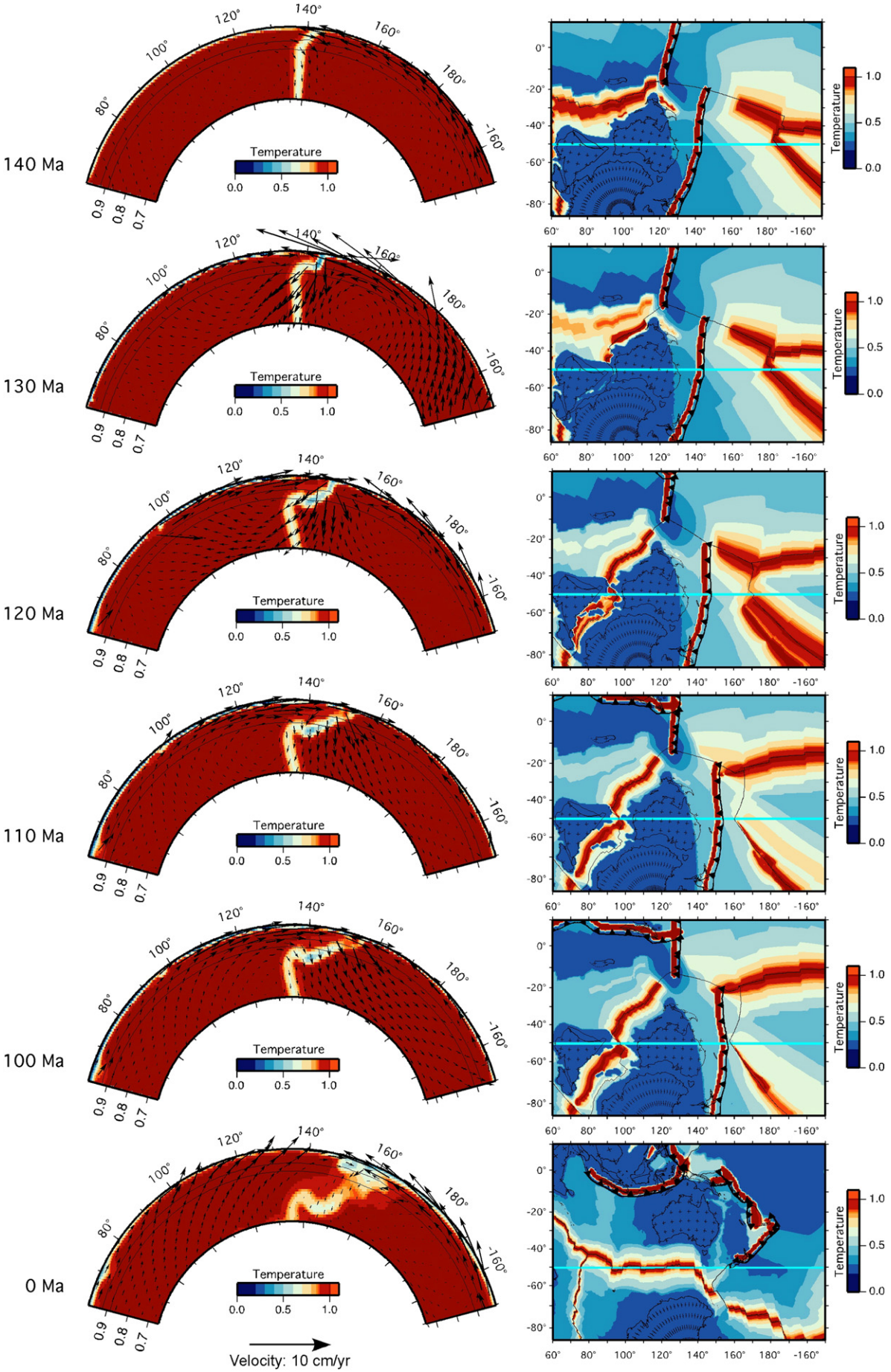
140 Ma
130 Ma
120 Ma
110 Ma
100 Ma
0 Ma
Temperature
0.0 0.5 1.0
Velocity: 10 cm/yr

Table 4
Initial model runs with subduction adjacent to reconstructed continental margin.

Model name	Rayleigh number (Ra)	Radial viscosities ($\eta_L, \eta_{UM}, \eta_{TZ}, \eta_{LM}$)	Initial temp. contrast	Slab depth (km)
RM[a]	1.3576×10^8	100, 1, 5, 50	0.5	~2000
RM_1	1.3576×10^8	100, 0.5, 5, 50	0.5	~2000
RM_2	1.3576×10^8	100, 0.25, 5, 50	0.5	~2000
RM_3	1.3576×10^8	100, 1, 5, 250	0.5	~2000
RM_4	2.7146×10^8	100, 1, 5, 50	0.5	~2000
RM_5	6.788×10^7	100, 1, 5, 50	0.5	~2000
RM_6	1.3576×10^8	100, 1, 5, 50	0.25	~2000

[a] 'Reference Model'.

Table 5
Second set of model runs with subduction translated 23° east of reconstructed continental margin.

Model name	Rayleigh number (Ra)	Radial viscosities ($\eta_L, \eta_{UM}, \eta_{TZ}, \eta_{LM}$)	Initial temp. contrast	Slab depth
Slab23E_RM	1.3576×10^8	100, 1, 5, 50	0.5	2230[a]
Slab23E_1	1.3576×10^8	100, 2, 10, 100	0.5	2230[a]
Slab23E_2	1.3576×10^8	100, 1, 30, 100	0.5	2230[a]
Slab23E_3	1.3576×10^8	100, 2, 50, 100	0.5	2230[a]

[a] Slab depth was extended in the later series of model runs to reflect long-lived subduction between Eastern Gondwanaland and the paleo-Pacific.

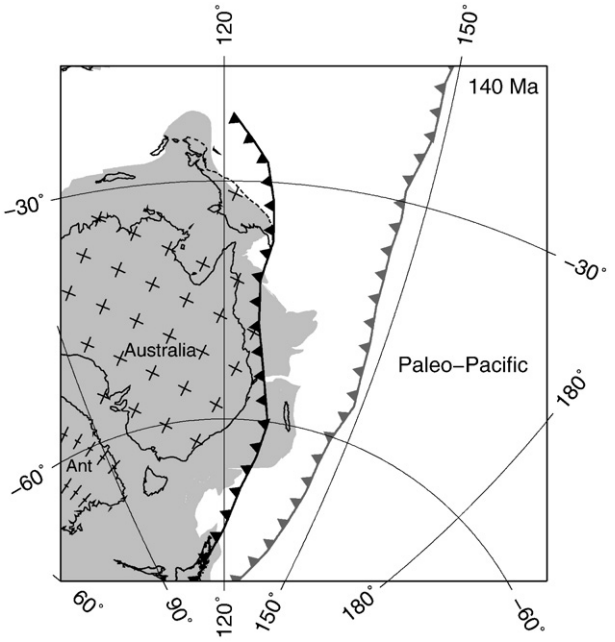

Fig. 4. Tectonic reconstruction of Australia at 140 Ma showing the location of the subduction zone used in the 'RM' model series (black) and the location of the subduction zone shifted 23° east (from the 'Slab23E' model series) (grey). Triangles point in the direction of the overriding plate. Grey shading represents the extent of present-day continental crust and has been included as a guide only. Ant – Antarctica.

volume of more shallowly penetrating high velocity material beneath the South Fiji Basin, at approximately 180°E (just west of the Tonga–Kermadec Trench), that extends to ~1200 km depth. It is inferred that cold subducted slabs produce these anomalous velocity signatures (Grand, 2002; Romanowicz, 2008; Zhao, 2009). Seismic tomography images also capture compositional variations (Romanowicz, 2008; Nakajima et al., 2009; Yamada et al., 2009; Zhao, 2009; Maruyama et al., 2009). In interpreting seismic tomography images of the southwest Pacific, knowledge of the tectonic history of the region increases our confidence in attributing the pattern of high velocity anomalies to slab material.

When Cretaceous subduction is adjacent to the paleo-continental margin the resultant present-day temperature structure of the mantle shows no cold material in the lower mantle beneath eastern Australia (Fig. 11B). The slab is confined to the upper mantle where it is laid out flat above the 660 km boundary, with limited penetration into the lower mantle. This presents a significant mismatch with the seismic inversions. Shifting subduction 23° east of eastern Australia in the Late Cretaceous allows the mantle to evolve with present-day slab material extending from the surface to deep in the lower mantle beneath eastern Australia (Fig. 11C). Thus the modelled present-day temperature structure is in closer agreement to seismic tomography. The majority of slab material is confined to the lower mantle, except where it has detached from the surface at ~150°E and traces remain in the upper mantle and transition zone. The current *CitcomS* models do not retain as much cold material in the upper mantle, as is inferred from the seismic tomography models. Increasing mantle viscosities resulted in a larger volume of slab material remaining at shallower depths in the mantle, however the models were unsuccessful in producing the distinct band of inferred cold material in the upper 660 km.

4. Discussion

Geodynamic modelling of the Australian region since 140 Ma predicts surface vertical motion in eastern Australia consistent with geological data. As the Australian plate moves eastward between 140 Ma and ~100 Ma, it overrides subducted oceanic lithosphere originating from subduction beneath Eastern Gondwanaland of the Phoenix plate, part of the paleo-Pacific Ocean (Panthalassa). As the subducting slab descends through the upper mantle it viscously drags down the overlying lithosphere, creating a broad region of negative dynamic topography in eastern Australia. This zone of deflection expands westward towards the continental interior between 140 and 100 Ma, covering the entire eastern half of the continent by 100 Ma. These results are in agreement with Gurnis et al. (1998), Gurnis et al. (2000), Waschbusch et al. (2009) and Korsch and Totterdell (2009) who have previously attributed Cretaceous subsidence in eastern Australian basins to mantle convection processes.

The geodynamic models with Cretaceous subduction 23° east of the reconstructed margin result in accelerated subsidence in the Eromanga and Surat basins at 120 Ma, in agreement with borehole data along an east to west transect ~27°S, between ~141°E and 152°E. This subsidence event coincides with a 4.5 cm/yr increase in the eastward velocity of the Australian plate (Fig. 12). As a result, the overriding Australian plate more rapidly moves across slab material that is descending at shallower depths in the mantle. The increase in the rate of subsidence occurs simultaneously in the two basins but at a slightly higher rate in the east, consistent with observations. Comparing the slopes of the modelled and geologically inferred subsidence curves reveals a high degree of similarity, highlighting that both timing and the rate of basin subsidence can be reproduced using geodynamic models.

4.1. Constraining the location of Cretaceous aged subduction east of Australia

Our assimilation of geological observations with geodynamic models strongly suggests that the Cretaceous subduction zone that paralleled eastern Australia was located up to ~1000 km offshore, ~23° east of the reconstructed continental margin. A combination of

Fig. 3. Mantle temperature cross-sections (~50°S) and regional temperature depth slices (88 km depth) at 10 Myr intervals during the Early to Mid-Cretaceous phase of basin subsidence, and at present day.

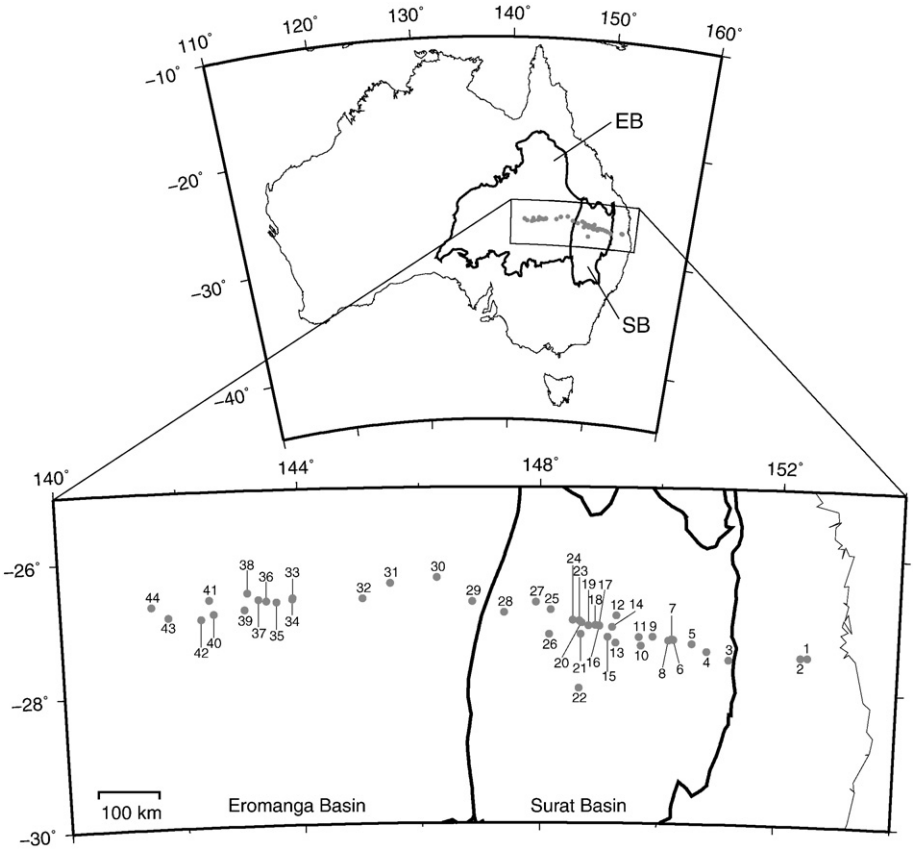

Fig. 5. Map of Australia showing the outlines of the Eromanga (EB) and Surat (SB) basins, and locations of boreholes used to calculate tectonic subsidence (grey dots). 1 – Lockrose 1; 2 – Baylem 1; 3 – Cecil Plains West 1; 4 – Kumbarilla 1; 5 – Alick Creek 1; 6 – Lorraine 1; 7 – Leichhardt 1; 8 – Arlington 1; 9 – Meandarra 1; 10 – Paloma 1; 11 – Coalbah 1; 12 – Apple Tree 1; 13 – Red Cap 1; 14 – Myall Creek 1; 15 – Grantham 1; 16 – Newington 1; 17 – Newington 2; 18 – Taralga 1; 19 – Kincora 1; 20 – Narelle 1; 21 – Basketyard Creek 1; 22 – Bainbilla 1; 23 – Avondale South 1; 24 – Tory Boy 2; 25 – Glenroy 1; 26 – Hoolah 1; 27 – Strathmore 1; 28 – Scalby 1; 29 – Lowood 1; 30 – Charleville 1; 31 – Quilberry 1; 32 – Quilpie 1; 33 – GSQ Eromanga 1; 34 – Mongarlo 1; 35 – Eromanga 1; 36 – Kenmore 1; 37 – Black Stump 1; 38 – Mount Bellalie 1; 39 – Berellem 1; 40 – Boldrewood 1; 41 – Mount Howitt 2; 42 – Wareena 1; 43 – Barrolka East 1; 44 – Cook North 1.

geodynamic modelling, tectonic subsidence analysis and seismic tomography analysis precludes subduction further west. In simulations with subduction adjacent to the continental margin, subsidence in the Eromanga and Surat basins accelerates 20 Myr earlier than inferred from well data. This time lag is consistently observed for a variety of mantle conditions, including different mantle viscosities, Rayleigh numbers and thermal conditions. A mismatch between the modelled present-day mantle temperature structure and mantle seismic tomography also arises when subduction is too far west. While S- and P-wave seismic tomography reveals anomalously high velocity material in the lower mantle beneath eastern Australia, inferred to represent slab material, these models do not predict slab material deeper than ~900 km in regions east of longitude ~130°E, and therefore beneath the Eromanga and Surat basins.

A convergent margin paralleled eastern Gondwanaland from as early as the Devonian (Murray et al., 1987), with evidence for subduction related magmatism preserved in the Lachlan Fold Belt and New England Orogen (Leitch, 1975; Cawood, 1982; McPhie, 1987; Murray et al., 1987; Little et al., 1992; Betts et al., 2002). Since at least the Late Paleozoic, the subduction zone that formed Australia's paleo-Pacific margin was mobile (Holcombe et al., 1997; Jenkins et al., 2002), yet the relative distance of the subduction zone from the continental edge for much of the Mesozoic has remained enigmatic.

The Paleozoic history of subduction has been well constrained by a combination of structural and geochemical investigations. The Late Paleozoic to early Triassic subduction zone was highly mobile (Jenkins et al., 2002). According to Jenkins et al. (2002), during the Early Carboniferous the subduction zone remained stationary at the continental margin, and fuelled volcanic eruptions of the New England Fold Belt, a volcanic arc at this time. This was followed by a phase of subduction zone retreat in the Late Carboniferous–Early Permian, inferred from lithospheric extension and back-arc magmatism. In the Late Permian the subduction zone began to advance back towards the paleo-coastline, expressed by compressional tectonics that initiated the Hunter-Bowen Orogeny and foreland basin loading, and re-established a magmatic arc. This advancement continued until the Early Triassic. By the Late Triassic, extension had recommenced in eastern Australia, forming elongate basins. Holcombe et al. (1997) even speculate that this extension may have been driven by slab rollback and oceanward migration of the subduction hinge.

These Paleozoic and Early Triassic trends support a distal subduction zone during the Cretaceous. Although it has been suggested that the Cretaceous margin of Australia was analogous to the present-day Chilean margin, with subduction adjacent to the continental margin (Veevers, 1984; Veevers, 2000), our geodynamic modelling results combined with indicators from the geological record suggest that this is unlikely. During the Early Cretaceous there is a lack of strong evidence for subduction zone magmatism in eastern Australia,

Table 6
Best fit, upper and lower values of ϕ_0 (porosity) and c (constant representing porosity decrease with depth), for each type of lithology, used to compute tectonic subsidence (Eq. (5)) (Gallagher, 1990).

	ϕ_0 (%)	c (km^{-1})	ϕ_0 (%)	c (km^{-1})	ϕ_0 (%)	c (km^{-1})	
Sandstone	43.0	0.718	48.0	0.567	38.0	0.987	2670
Siltstone	45.7	1.158	51.0	0.965	41.0	1.310	2680
Shale	50.4	1.616	55.0	1.300	45.0	1.760	2680

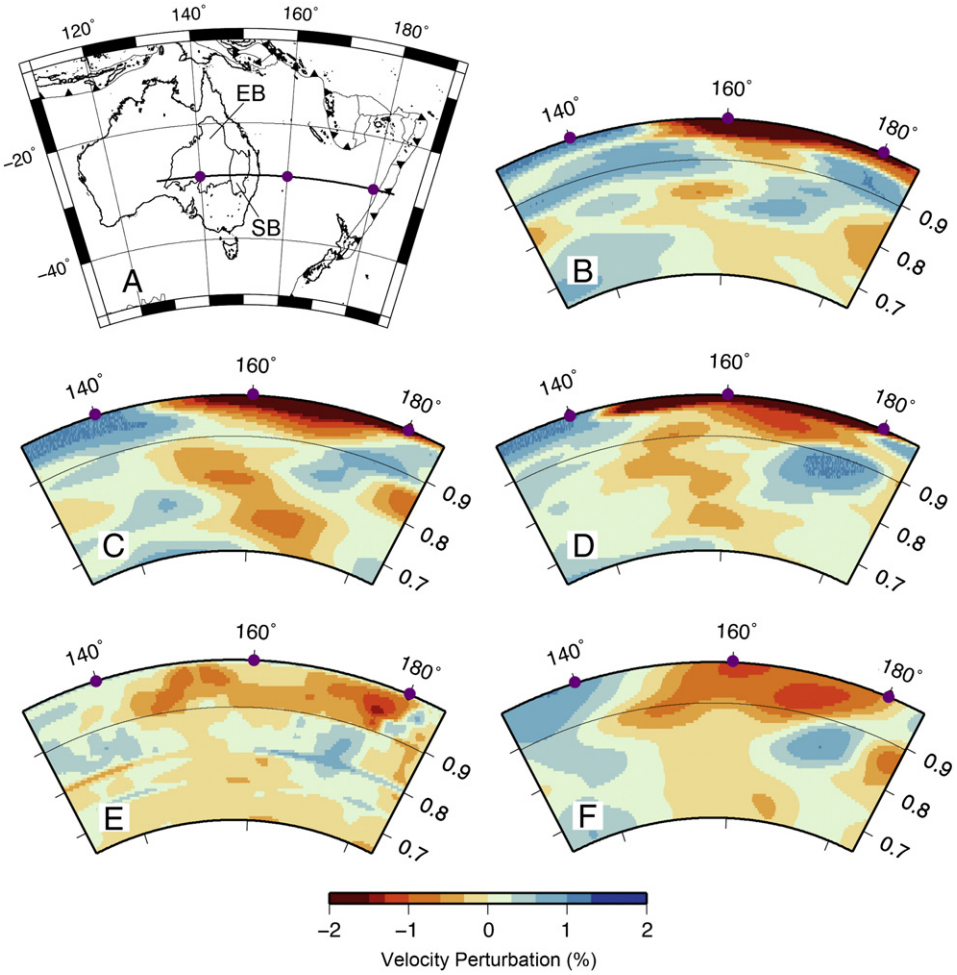

Fig. 6. Location map showing profiles of seismic tomography at 25°S, through the Eromanga and Surat basins (A), and seismic tomography cross-sections to 2230 km depth (B–F). S-wave models are (B) S20RTS (Ritsema et al., 1999), (C) TX2007 (Simmons et al., 2007) and (D) TXBW (Grand 2002), and P-wave models are (E) MITP08 (Li et al., 2008) and (F) PRI-P05 (Montelli et al., 2006). Anomalously fast velocities (blue areas) are inferred to represent cold regions of the mantle, and anomalously slow velocities (red areas) are inferred to represent hot regions. EB – Eromanga Basin; SB – Surat Basin.

yet during the Carboniferous and Late Permian, when subduction is inferred to have been adjacent to the paleo-coastline, there is abundant geological evidence for arc volcanism and convergent margin tectonics such as foreland basin loading and orogeny. Although there are volcanogenic sediments preserved in the Eromanga and Surat basins, there is strong evidence to suggest that they have an extensional origin. Ewart et al. (1992) and Bryan et al. (1997) describe a large-scale extensional volcanic event in the Whitsundays Volcanic Province (offshore northeast Queensland) 120–105 Ma. Volcanic debris was distributed thousands of kilometres inland by wind and paleo-rivers, as far south as the Otway and Gippsland basins off Australia's southern margin (Bryan et al., 1997; Norvick et al., 2001).

Geodynamic modelling of Cretaceous subduction 23° east of the reconstructed eastern Australian margin successfully predicts accelerated subsidence in the Eromanga and Surat basins at 120 Ma. These findings are in agreement with well data and seismic tomography, and are consistent with earlier Late Paleozoic–Early Triassic subduction trends in eastern Australia (Holcombe et al., 1997; Jenkins et al., 2002). These results further reveal that estimates of the timing of subsidence depend critically on plate kinematic reconstructions.

5. Conclusions

We demonstrate that geodynamic models driven by plate kinematics and linked to geological and geophysical observations, can be used to test alternative plate boundary scenarios and unravel the driving mechanisms and history of intracontinental basin evolution. Our results have constrained the location of the subduction zone that paralleled Eastern Gondwanaland during the Cretaceous to approximately 23° east of the reconstructed continental margin, simulating a large back-arc basin. The subduction zone at this time was therefore located east of Gondwanaland's margin by more than 1000 km. When this plate boundary configuration is assimilated into geodynamic forward models of the Australian region since 140 Ma, Early Cretaceous accelerated subsidence in the Eromanga and Surat basins in eastern Australia is reproduced consistent with geological data. The modelled present-day mantle beneath eastern Australia, and as far east as the South Fiji Basin, matches S- and P-wave seismic tomography models. This highlights the temporal and spatial robustness of the model.

We have demonstrated that geodynamic models, coupled with high-performance computing, enable the development of “holistic” earth models that reconcile deep Earth structure with plate boundary reconstructions and geological observations such as tectonic subsidence and basin stratigraphy. The workflow we have used is adaptable, and applying it to other regions of the globe will facilitate attempts to constrain plate boundary reconstructions elsewhere in time and space.

Acknowledgement

We would like to thank Kerry Gallagher for providing us with well data for the Eromanga and Surat basins. MG was supported by the National Science Foundation under EAR-0810303.

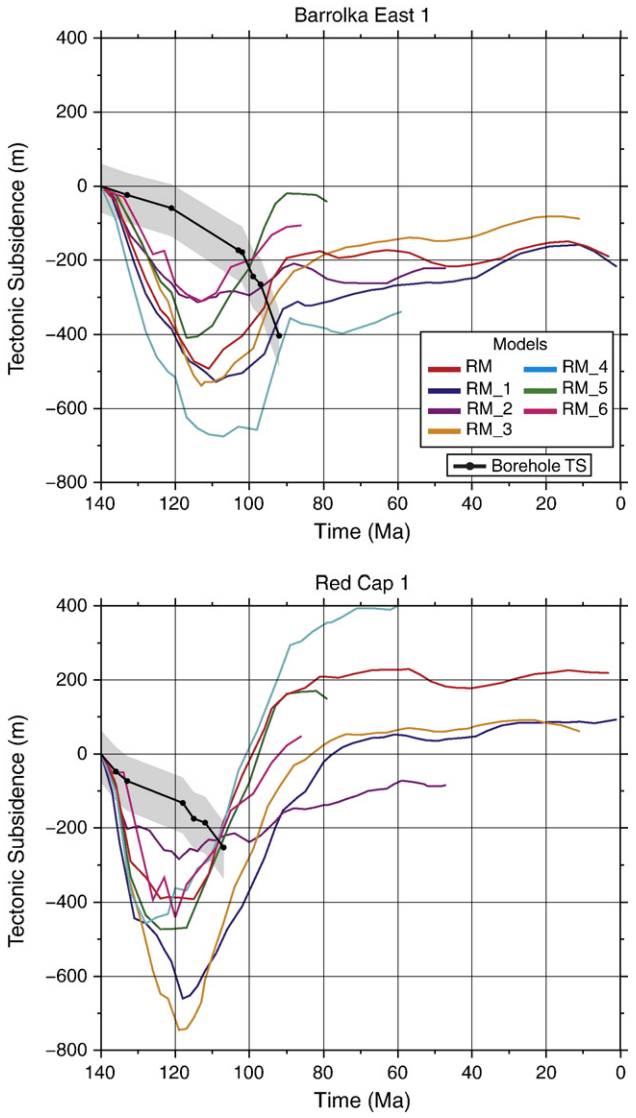

Fig. 7. Modelled (coloured lines) and 'observed' (black line with grey error polygon) tectonic subsidence for Barrolka East 1 and Red Cap 1 during the Cretaceous. Models are from the RM model series (see Table 4 for model parameters). Note: Not all *CitcomS* models were solved to present-day and this is why the coloured lines stop at different ages.

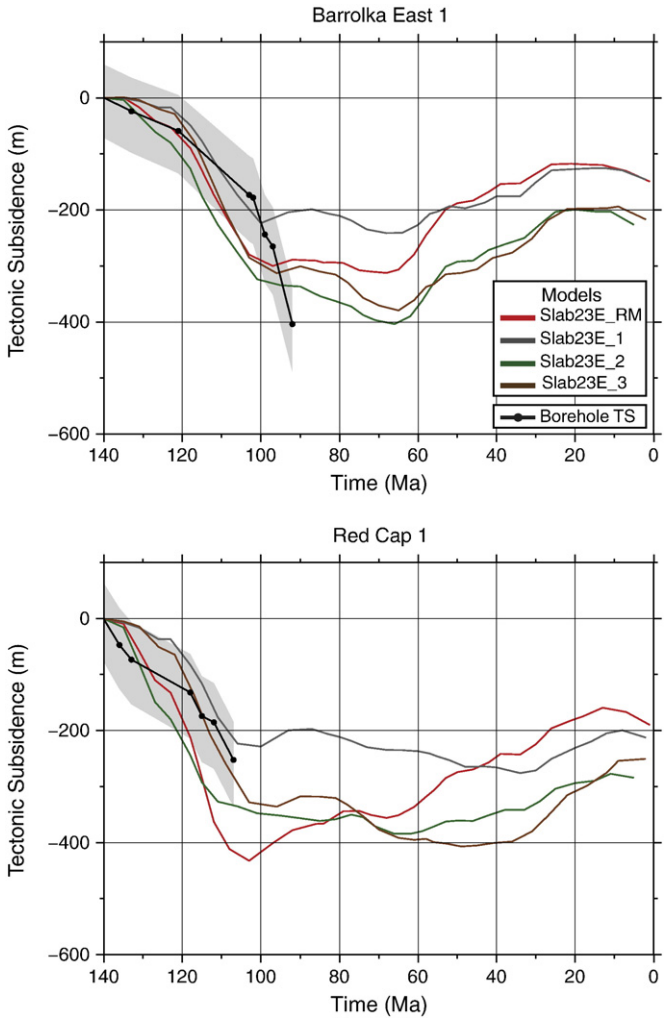

Fig. 8. Modelled (coloured lines) and 'observed' (black line with grey error polygon) tectonic subsidence for Barrolka East 1 and Red Cap 1 during the Cretaceous. Models are from the Slab23E model series (see Table 5 for model parameters). Note: Not all *CitcomS* models were solved to present-day and this is why the coloured lines stop at different ages.

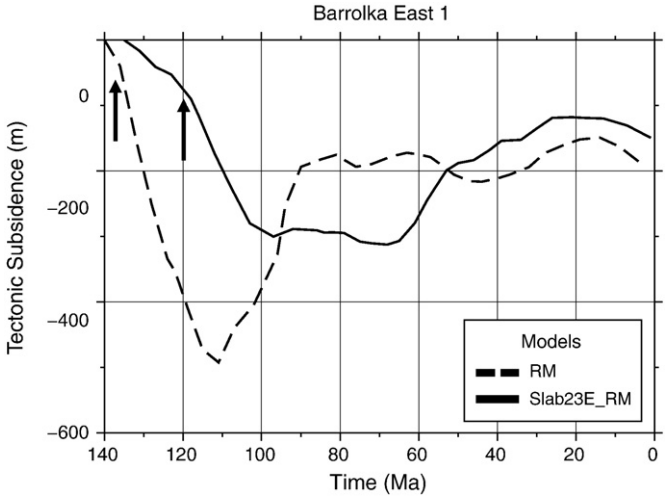

Fig. 9. Model subsidence curves for Barrolka East 1 in the Eromanga Basin, for models RM (dashed line) and Slab23E_RM (solid line). Arrows indicate the onset of increased subsidence, illustrating the ~20 Myr difference in timing.

References

Baker-Hebert, L., Antoshechkina, P., Asimow, P., Gurnis, M., 2009. Emergence of a low-viscosity channel in subduction zones through the coupling of mantle flow and thermodynamics. Earth and Planetary Science Letters 278, 243–256.

Betts, P.G., Giles, D., Lister, G.S., Frick, L.R., 2002. Evolution of the Australian lithosphere. Australian Journal of Earth Sciences: An International Geoscience Journal of the Geological Society of Australia 49, 661–695.

Billen, M.I., Gurnis, M., 2001. A low viscosity wedge in subduction zones. Earth and Planetary Science Letters 193, 227–236.

Billen, M.I., Gurnis, M., Simons, M., 2003. Multiscale dynamics of the Tonga–Kermadec subduction zone. Geophysical Journal International 153, 359–388.

Boyden, J., Müller, R.D., Gurnis, M., Torsvik, T., Clark, J., Turner, M., Ivey-Law, H., Farrow, J., Watson, R. in press. Next-generation plate-tectonic reconstructions using GPlates. Keller, G.R., Baru, C., (Ed.). Geoinformatics: Cyberinfrastructure for the Solid Earth Sciences Cambridge University Press, Cambridge.

Bryan, S.E., Constantine, A.E., Stephens, C.J., Ewart, A., Schön, R.W., Parianos, J., 1997. Early Cretaceous volcano-sedimentary successions along the eastern Australian continental margin: implications for the break-up of eastern Gondwana. Earth and Planetary Science Letters 153, 85–102.

Cawood, P.A., 1982. Structural relations in the subduction complex of the paleozoic New England Fold Belt, Eastern Australia. The Journal of Geology 90, 381–392.

Christensen, U.R., 1996. The influence of trench migration on slab penetration into the lower mantle. Earth and Planetary Science Letters 140, 27–39.

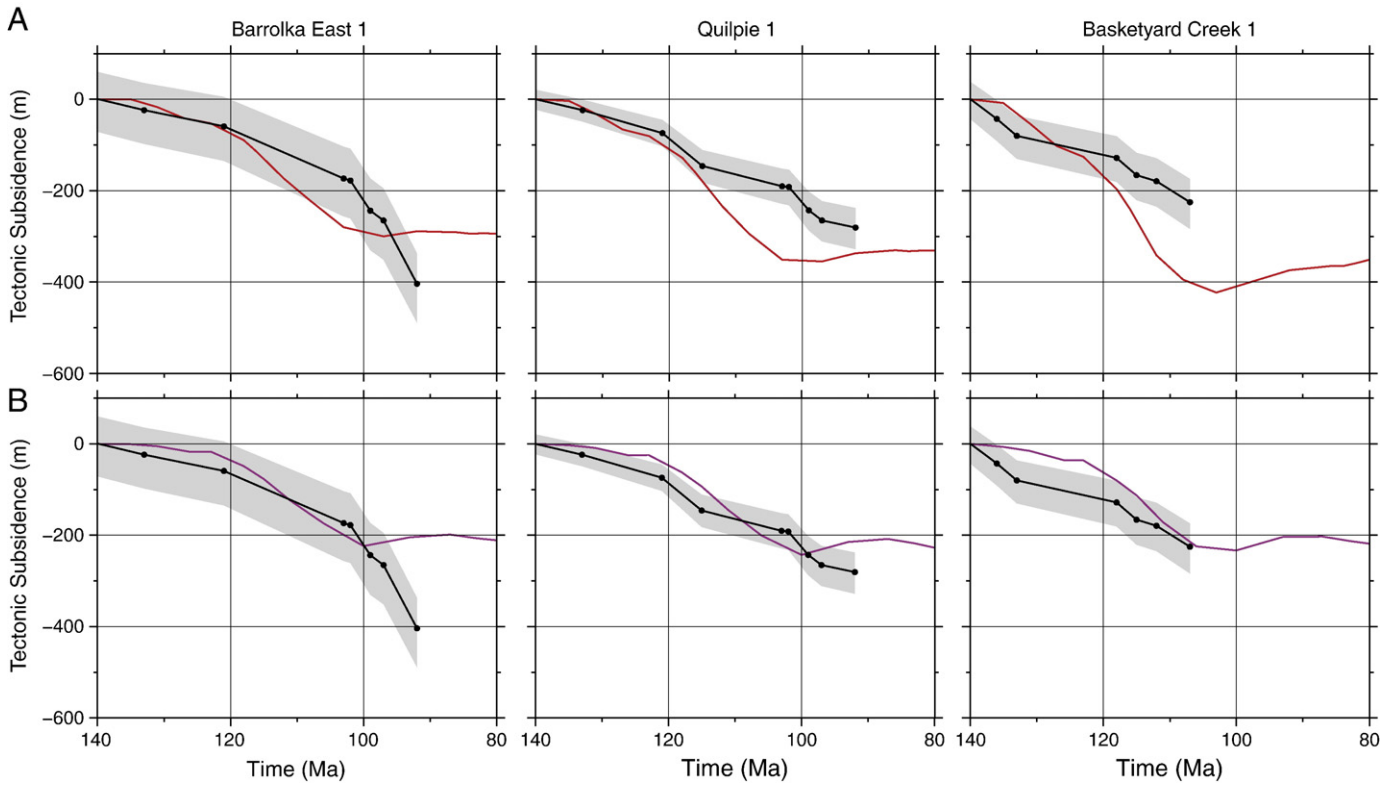

Fig. 10. Modelled and 'observed' tectonic subsidence for Barrolka East 1, Quilpie 1 and Basketyard Creek 1 during the Cretaceous, for models Slab23E_RM (A) and Slab23E_1 (B). Comparing the results for each well location reveals that model Slab23E_1 produces a better fit between the observed and predicted rates of subsidence from 140 Ma. See Table 5 for model parameters.

DiCaprio, L., 2009. The Geodynamic History of the Australian Region Since the Cretaceous. Doctor of Philosophy, The University of Sydney.

DiCaprio, L., Gurnis, M., Müller, R.D., 2009. Long-wavelength tilting of the Australian continent since the Late Cretaceous. Earth and Planetary Science Letters 278, 175–185.

Ewart, A., Schon, R.W., Chappell, B.W., 1992. The Cretaceous volcanic-plutonic province of the central Queensland (Australia) coast – a rift related 'calc-alkaline' province. Transactions of the Royal Society of Edinburgh. Earth Sciences 83, 327–345.

Exon, N.F., Senior, B.R., 1976. The Cretaceous of the Eromanga and Surat Basins. Bureau of Mineral Resources Journal of Australian Geology and Geophysics 1, 33–50.

Gallagher, K., 1990. Permian to Cretaceous subsidence history along the Eromanga-Brisbane Geoscience Transect. In: Finlayson, D.M. (Ed.), The Eromanga-Brisbane Geoscience Transect: A guide to basin development across Phanerozoic Australia. Southern Queensland Bureau of Mineral Resources, Australia, pp. 133–151.

Gallagher, K., Lambeck, K., 1989. Subsidence, sedimentation and sea-level changes in the Eromanga Basin, Australia. Basin Research 2, 115–131.

Gallagher, K., Dumitru, T.A., Gleadow, A.J.W., 1994. Constraints on the vertical motion of eastern Australia during the Mesozoic. Basin Research 6, 77–94.

Grand, S.P., 2002. Mantle shear-wave tomography and the fate of subducted slabs. Philosophical Transactions of the Royal Society of London. Series A: Mathematical, Physical and Engineering Sciences 360, 2475–2491.

Gurnis, M., 1990. Bounds on global dynamic topography from Phanerozoic flooding of continental platforms. Nature 344, 754–756.

Gurnis, M., 1992. Rapid continental subsidence following the initiation and evolution of subduction. Science 255, 1556.

Gurnis, M., Müller, R.D., Moresi, L., 1998. Cretaceous vertical motion of Australia and the Australian–Antarctic Discordance. Science 279, 1499–1504.

Gurnis, M., Moresi, L., Müller, R.D., 2000. Models of mantle convection incorporating plate tectonics: the Australian region since the Cretaceous. In: Richards, M.A., Gordon, R., Van Der Hilst, R. (Eds.), The History and Dynamics of Global Plate Motions. American Geophysical Union, Washington D.C, pp. 211–238.

Gurnis, M., Turner, M., DiCaprio, L., Spasojević, S., Müller, R.D., Boyden, J., Seton, M., Manea, V.C., Bower, D.J. 2009. Global Plate Reconstructions with Continuously Closing Plates. Geochemistry, Geophysics, Geosystems, submitted.

Hager, B., 1984. Subducted slabs and the geoid: constraints on mantle rheology and flow. Journal of Geophysical Research 89 (B7), 6003–6016.

Haq, B.U., Hardenbol, J., Vail, P.R., 1987. Chronology of fluctuating sea levels since the Triassic. Science 235, 1156–1167.

Holcombe, R.J., Stephens, C.J., Fielding, C.R., Gust, D., Little, T.A., Sliwa, R., Kassan, J., Mcphie, J., Ewart, A. (Eds.), 1997. Tectonic evolution of the northern New England Fold Belt: The Permian–Triassic Hunter–Bowen event: Geological Society of Australia, Special Publication, 19.

Jenkins, R.B., Landenberger, B., Collins, W.J., 2002. Late Palaeozoic retreating and advancing subduction boundary in the New England Fold Belt, New South Wales. Australian Journal of Earth Sciences 49, 467–489.

Korsch, R.J., Totterdell, J.M., 2009. Subsidence history and basin phases of the Bowen, Gunnedah and Surat Basins, eastern Australia. Australian Journal of Earth Sciences 56, 335–353.

Leitch, E.C., 1975. Plate tectonic interpretation of the paleozoic history of the New England Fold Belt. Geological Society of America Bulletin 86, 141–144.

Li, C., van der Hilst, R.D., Engdahl, E.R., Burdick, S., 2008. A new global P wave speed variations in Earth's mantle. Geochemistry, Geophysics, Geosystems 9, Q05018. doi:10.1029/2007GC001806.

Lithgow-Bertelloni, C., Gurnis, M., 1997. Cenozoic subsidence and uplift of continents from time-varying dynamic topography. Geology 25, 735–738.

Little, T.A., Holcombe, R.J., Gibson, G.M., Offler, R., Gans, P.B., Mcwilliams, M.O., 1992. Exhumation of late Paleozoic blueschists in Queensland, Australia, by extensional faulting. Geology 20, 231–234.

Manea, V.C., Gurnis, M., 2006. Central Mexican Subduction zone evolution controlled by a low viscosity mantle wedge. Eos Trans. AGU 87 (52) Fall Meet. Suppl., Abstract T13F-03.

Manea, V., Gurnis, M., 2007. Subduction zone evolution and low viscosity wedges and channels. Earth and Planetary Science Letters 264, 22–45.

Maruyama, S., Hasegawa, A., Santosh, M., Kogiso, T., Omori, S., Nakamura, H., Kawai, K., Zhao, D., 2009. The dynamics of big mantle wedge, magma factory, and metamorphic–metasomatic factory in subduction zones. Gondwana Research 414–430.

McNamara, A.K., Zhong, S., 2004. Thermochemical structures within a spherical mantle: Superplumes or piles? Journal of Geophysical Research 109, B07402. doi:10.1029/2003JB002847.

McPhie, J., 1987. Andean analogue for the Late Carboniferous volcanis arc and arc flank environments of the western New England Orogen, New South Wales, Australia. Tectonophysics 138, 269–288.

Mitrovica, J.X., Beaumont, C., Jarvis, G.T., 1989. Tilting of continental interiors by the dynamical effects of subduction. Tectonics 8, 1079–1094.

Montelli, R., Nolet, G., Dahlen, F.A., Masters, G., 2006. A catalogue of deep mantle plumes: new results from finite-frequency tomography. Geochemistry, Geophysics, Geosystems 7, Q11007. doi:10.1029/2006GC001248.

Müller, R.D., Sdrolias, M., Gaina, C., Roest, W.R., 2008a. Age, spreading rates, and spreading asymmetry of the world's ocean crust. Geochemistry, Geophysics, Geosystems 9, Q04006. doi:10.1029/2007GC001743.

Müller, R.D., Sdrolias, M., Gaina, C., Steinberger, B., Heine, C., 2008b. Long-term sea-level fluctuations driven by ocean basin dynamics. Science 319, 1357–1362.

Murray, C.G., Fergusson, C.L., Flood, P.G., Whitaker, W.G., Korsch, R.J., 1987. Plate tectonic model for the Carboniferous evolution of the New England Fold Belt.

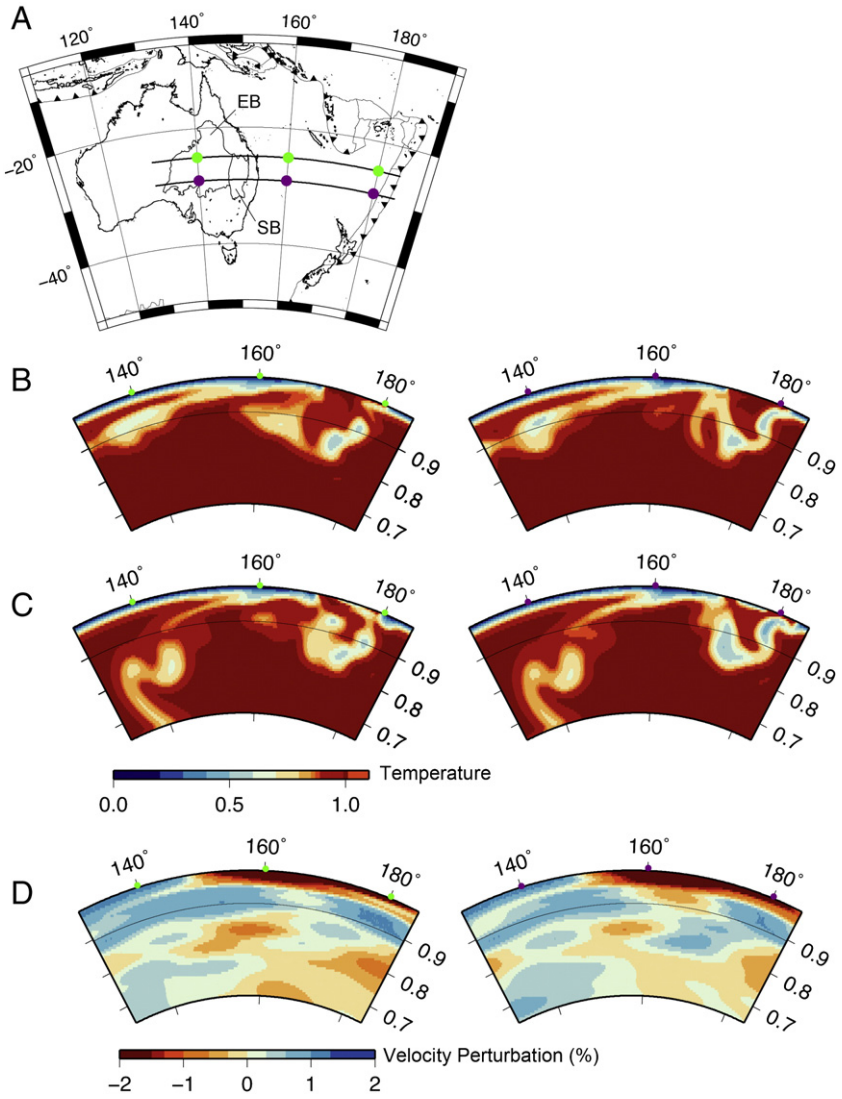

Fig. 11. Location map showing profiles of *CitcomS* modelled temperature, and seismic tomography at 25°S and 29°S (A), modelled mantle temperature cross-sections (B–C) and S-wave seismic tomography cross-sections (model S20RTS – Ritsema et al., 1999) (D). Temperature profiles for the reference model (model RM) reveal cold slab material penetrating to ~1200 km, with the majority in the upper mantle and transition zone (B). When the subduction zone is shifted east (model Slab23E_RM) slab material penetrates to deep in the lower mantle beneath eastern Australia, with a majority of cold material between ~700 and 1600 km depth (C). In both models, a second mass of cold slab material penetrates to ~1200 km depth, west of the Tonga–Kermadec Trench.

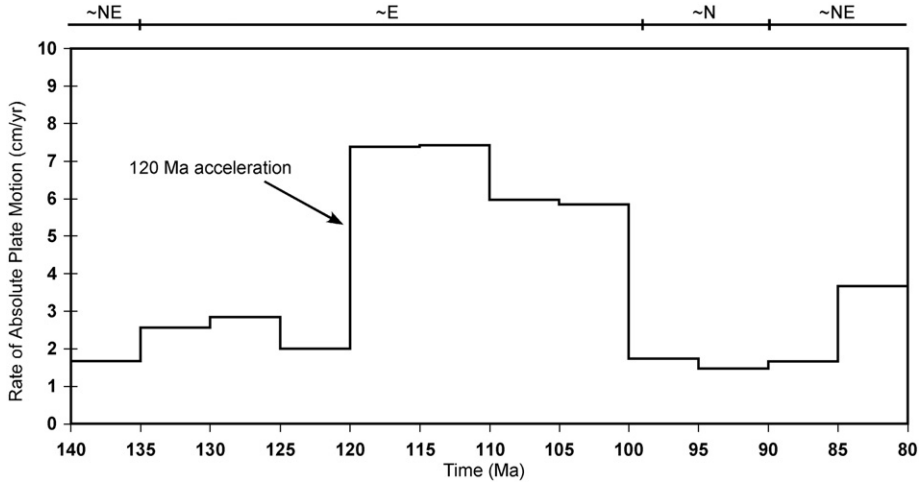

Fig. 12. Rate of absolute motion of the Australian plate from 140–80 Ma; averaging interval is 5 Myr. The approximate direction of plate movement is labelled for different intervals during this timeframe (annotated line above graph).

Australian Journal of Earth Sciences: An International Geoscience Journal of the Geological Society of Australia 34, 213–236.
Nakajima, J., Tsuji, Y., Hasegawa, A., Kita, S., Okada, T., Matsuzawa, T., 2009. Tomographic imaging of hydrated crust and mantle in the subducting Pacific slab beneath Hokkaido, Japan: evidence for dehydration embrittlement as a cause of intraslab earthquakes. Gondwana Research 16, 470–481.
Norvick, M.S., Smith, M.A., Power, M.R., 2001. The plate tectonic evolution of Eastern Australasia guided by the stratigraphy of the Gippsland Basin. In: Hill, K.C., Bernecker, T. (Eds.), Eastern Australasian Basins Symposium, A Refocused Energy Perspective for the Future: Petroleum Exploration Society of Australia, Special Publication, pp. 15–23.
Peacock, S.M., 1990. Fluid processes in subduction zones. Science 248, 329–337.
Ranero, C.R., Phipps-Morgan, J., Mcintosh, K., Reichert, C., 2003. Bending-related faulting and mantle serpentinization at the Middle America trench. Nature 425, 367–373.
Raza, A., Hill, K.C., Korsch, R.J., 2009. Mid-Cretaceous uplift and denudation of the Bowen and Surat Basins, eastern Australia: relationship to Tasman Sea rifting from apatite fission-track and vitrinite-reflectance data. Australian Journal of Earth Sciences 56, 501–531.
Ritsema, J., van Heijst, H.J., Woodhouse, J.H., 1999. Complex shear wave velocity structure imaged beneath Africa and Iceland. Science 286, 1925–1928.
Romanowicz, B., 2008. Using seismic waves to image Earth's internal structure. Nature 451, 266–268.
Russell, M., Gurnis, M., 1994. The planform of epeirogeny: vertical motions of Australia during the Cretaceous. Basin Research 6, 63–76.
Sandiford, M., 2007. The tilting continent: a new constraint on the dynamic topographic field from Australia. Earth and Planetary Science Letters 261, 152–163.
Schellart, W.P., Lister, G.S., Toy, V.G., 2006. A Late Cretaceous and Cenozoic reconstruction of the Southwest Pacific region: tectonics controlled by subduction and slab rollback processes. Earth-Science Reviews 76, 191–233.
Simmons, N.A., Forte, A.M., Grand, S.P., 2007. Thermochemical structure and dynamics of the African superplume. Geophysical Research Letters 34, L02301. doi:10.1029/2006GL028009.
Spasojević, S., Liu, L., Gurnis, M., Müller, R.D., 2008. The case for dynamic subsidence of the United States east coast since the Eocene. Geophysical Research Letters 35, L08305. doi:10.1029/2008GL033511.
Stevenson, D.J., Turner, J.S., 1977. Angle of subduction. Nature 270, 334–336.
Tan, E., Gurnis, M., Han, L., 2002. Slabs in the lower mantle and their modulation of plume formation. Geochemistry, Geophysics, Geosystems 3 (11), 1067. doi:10.1029/2001GC000238.
Tan, E., Choi, E., Thoutireddy, P., Gurnis, M., Aivazis, M., 2006. GeoFramework: Coupling multiple models of mantle convection within a computational framework. Geochemistry, Geophysics, Geosystems 7, Q06001. doi:10.1029/2005GC001155.
Tatsumi, Y., Sakuyama, M., Fukuyama, H., Kushiro, I., 1983. Generation of arc basalt magmas and thermal structure of the mantle wedge in subduction zones. Journal of Geophysical Research 88 (B7), 5815–5825.
Tovish, A., Schubert, G., Luyendyk, B., 1978. Mantle flow pressure and the angle of subduction: non-Newtonian corner flows. Journal of Geophysical Research 83 (B12), 5892–5898.
Veevers, J.J., 1984. Phanerozoic Earth History of Australia. Oxford University Press, New York.
Veevers, J.J., 2000. Billion-year earth history of Australia and neighbours in Gondwanaland, North Ryde. Gemoc Press, N.S.W.
Veevers, J.J., 2006. Updated Gondwana (Permian–Cretaceous) earth history of Australia. Gondwana Research 9, 231–260.
Waschbusch, P., Korsch, R.J., Beaumont, C., 2009. Geodynamic modelling of aspects of the Bowen, Gunnedah, Surat and Eromanga Basins from the perspective of convergent margin processes. Australian Journal of Earth Sciences 56, 309–334.
Yamada, A., Zhao, D., Inoue, T., Suetsugu, D., Obayashi, M., 2009. Seismological evidence for compositional variations at the base of the mantle transition zone under Japan Islands. Gondwana Research 16, 482–490.
Zhao, D., 2009. Multiscale seismic tomography and mantle dynamics. Gondwana Research 15, 297–323.
Zhong, S., Zuber, M.T., Moresi, L., Gurnis, M., 2000. Role of temperature-dependent viscosity and surface plates in spherical shell models of mantle convection. Journal of Geophysical Research 105 (B5), 11063–11082.